Acta Crystallographica Section B
Structural Science
ISSN 0108-7681

Variable-temperature crystal structure studies of *m*-nitroaniline

Grażyna Wójcik* and Jolanta Holband

Institute of Physical and Theoretical Chemistry, Wrocław University of Technology, Wyb. Wyspiańskiego 27, 50-370 Wrocław, Poland

Correspondence e-mail: wojcik@kchf.ch.pwr.wroc.pl

Received 16 June 2000
Accepted 19 March 2001

The crystal structure of *m*-nitroaniline has been examined at several temperatures over the 90–350 K range. Thermal evolution of the lattice parameters reveals a weak anomaly at 110 K and an important one at 300 K. The thermal expansion coefficients have been calculated at several temperatures and the principal axes cross-sections of the tensor were drawn. The lattice contraction along the *b* axis direction has been observed. The rigid-body analysis including an attached rigid group has provided the values of the translation and libration tensors at temperatures studied. The results indicate that *m*-nitroaniline undergoes a glass transition around 130 K arising from freezing molecular librations and translations. From above 340 K the growing plasticity of the *m*-nitroaniline crystal results in the loss of X-ray diffraction reflections. This is probably a second-order phase transition. It is coupled with a considerable increase in the nitro group torsion amplitude, but the NH$\cdots$O hydrogen bonds are preserved. Analysis of the temperature evolution of short intermolecular distances enabled us to consider the occurrence of reorienting aggregates of hydrogen-bonded molecules in the high-temperature plastic phase.

1. Introduction

Several papers dealing with crystallographic characterization of nitrobenzene derivatives were published recently. Among them there were two papers which discussed the two main modes, stack and pseudo-herringbone, in which nitrobenzene derivatives crystallize (André *et al.*, 1997*a*,*b*). The authors profited from crystal structures retrieved from the Cambridge Structural Database and emphasized the important role of weak interactions in the last packing mode. Allen, Baalham *et al.*, (1997) and Allen, Lommerse *et al.*, (1997) studied acceptor properties of nitro O atoms, which can be involved in intermolecular interactions with the hydroxyl group and halogen atoms. The combined crystallographic database and quantum-chemical *ab initio* investigation characterized these interactions both geometrically and energetically.

The order–disorder phase transition in *p*-chloronitrobenzene was studied by nuclear quadrupole resonance, differential thermal analysis (Meriles *et al.*, 1996) and adiabatic calorimetry (Tozuka *et al.*, 2000). It was shown that the disordered phase can exist outside the range of stability as a metastable phase and undergoes a glass transition arising from freezing of some molecular reorientations.

m-Nitroaniline has been the subject of numerous studies mainly because of its optical non-linearity (Davidov *et al.*,

1970; Southgate & Hall, 1971). Its crystal structure at room temperature has been found to be: $Pbc2_1$, a = 6.499 (1), b = 19.369 (4), c = 5.084 (1) Å, Z = 4 (Skapski & Stevenson, 1973; Ploug-Sørensen & Krogh Andersen, 1986). Some very weak intermolecular NH···O and CH···O hydrogen bonds (∼3.3–3.5 Å) extend roughly along the [101] and [10$\bar{1}$] directions. They form infinite molecular chains. Two adjacent chains form a molecular strand through other NH···O hydrogen bonds. The strands are packed crosswise on the (010) plane. Short distances (∼3.5 Å) occur between molecules translated along the c-axis direction forming the stacks of molecular chains. Fig. 1 shows the molecular packing in the *m*-nitroaniline crystal viewed roughly along the twofold screw axis. Molecular packing and the hydrogen-bond network in nitroanilines were discussed in the paper by Panunto *et al.* (1987). Their analysis of numerous crystal structures resulted in the conclusion that *m*- and *p*-nitroanilines prefer to form infinite molecular chains through sometimes very weak NH···O and CH···O intermolecular hydrogen bonds. The quantum-chemical studies of these interactions with semi-empirical methods carried for *m*- and *p*-nitroaniline enabled the conclusion that slightly different packings within the hydrogen-bonded molecular chains are energetically indistinguishable (Turi & Dannenberg, 1996). Recently, neutron diffraction studies of *m*-nitroaniline and 2-methyl-5-nitroaniline revealed the non-planarity of amino groups and the acceptor abilities of amino nitrogen, which result in the formation of molecular layers through NH···N interactions in the *m*-nitroaniline crystal (Goeta *et al.*, 1999).

The above and other interesting properties of *m*-nitroaniline, *i.e.* the sign reversal of the pyrroelectric coefficient at ∼140 K (Giermańska, 1984; Asaji & Weiss, 1985) and the occurrence of vibronic couplings in the vibrational spectra (Szostak, 1979, 1982, 1988; Szostak *et al.*, 1994), inspired us to investigate this crystal more thoroughly over a wide temperature range. Our recent paper (Szostak *et al.*, 1998) discussed molecular motions as studied with relaxation (proton NMR, dielectric measurements) and calorimetric (DSC) methods. These variable-temperature studies have revealed that *m*-nitroaniline also undergoes transformations below and above ambient conditions. DSC curves showed an anomaly at ∼140 K in cooling and heating cycles. This anomaly was similar to those corresponding to glass transitions (Höhne *et al.*, 1995). On the other hand, a weak singularity was found on heating and cooling curves at ∼363 K. The DSC heat-flow effect was tiny, but it could be correlated with the solid-state ^{1}H NMR, dielectric (Szostak *et al.*, 1998) and dilatometric (Szostak *et al.*, 1993) results. The decrease of the NMR-line second moment was related to 180° jumps of the amino protons. The onset of these jumps was situated at ∼320 K. The temperature dependences of the dielectric permittivity measured at variable frequencies revealed the appearance of a diffusionally disordered phase from above 363 K. Last but not least the direct dilatometric measurements of single-crystal specimens showed a weak singularity at 330 K.

All these experimental results are at the origin of this work. Crystal structure studies in the wide temperature range were performed with the aim of checking the crystal structure of *m*-nitroaniline below the low-temperature anomaly and above the high-temperature one. We also wanted to explore the thermal evolution of the crystal structure parameters, of the anisotropic thermal expansion coefficients and of the atomic displacement parameters. The rigid-body analysis was performed in order to try to compare the molecular dynamics found with the results of NMR, dielectric and Raman and far-IR (Szostak, 1982) investigations.

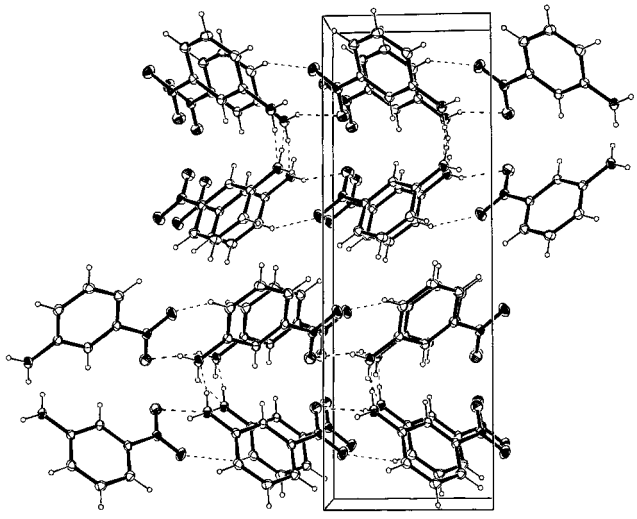

Figure 1
*ORTEP*3 (Farrugia, 1997) view of molecular packing in the *m*-nitroaniline crystal along the twofold screw axis.

2. Experimental

m-Nitroaniline purchased from 'REACHIM' was purified by multiple zone refinement. Single crystal specimens suitable for X-ray diffraction were grown from acetone/cyclohexane solution. The X-ray diffraction experiments were performed on a Kuma Diffraction four-circle automatic diffractometer equipped with an area detector and an Oxford Cryosystem cooling unit. Mo $K\alpha$ radiation (λ = 0.71073 Å) was used. The measurements were carried at 15 different temperatures in the 90–350 K range for four different crystal specimens measured at the following temperatures, respectively: 90 K; 110, 130, 160, 200, 240, 280, 300 and 320 K; 140, 180, 220 and 260 K; 302, 340 and 350 K. The precision of the temperature stability was 0.1°. The *m*-nitroaniline ($C_6H_6N_2O_2$, M = 138.13) crystals were yellow. In all the temperatures used the space group was $Pca2_1$ with four molecules in the unit cell. During the data collection ω scans were performed. No absorption corrections were applied. Data reductions were performed with Kuma *KM4CCD* software (Kuma Diffraction, 1999). The structures were solved by direct methods and refined by least-squares with the programs from the *SHELX*97 package (Sheldrick, 1990, 1997). Atomic scattering factors were taken from the *International Tables for Crystallography* (1992, Vol. C, Tables 4.2.6.8 and 6.1.1.4). The H atoms were found geometrically and refined isotropically. Other details of the data collection

Table 1
Experimental details.

Crystal data	
Chemical formula	$C_6H_6N_2O_2$
Chemical formula weight	138.13
Cell setting, space group	Orthorhombic, $Pca2_1$
a, b, c (Å)	18.873 (2), 6.5212 (9), 4.9980 (7)
V (Å^3)	615.13 (14)
Z	4
D_x (Mg m^{-3})	1.492
Radiation type	Mo $K\alpha$
No. of reflections for cell parameters	1415
θ range (°)	3.38–28.16
μ (mm^{-1})	0.115
Temperature (K)	110 (2)
Crystal form, colour	Plate, yellow
Crystal size (mm)	1.02 × 0.67 × 0.18
Data collection	
Diffractometer	Kuma Diffraction KM4CCD
Data collection method	ω scans
No. of measured, independent and observed parameters	4413, 1357, 1305
Criterion for observed reflections	$I > 2\sigma(I)$
R_{int}	0.0253
θ_{max} (°)	29.57
Range of h, k, l	$-26 \rightarrow h \rightarrow 25$ $-9 \rightarrow k \rightarrow 8$ $-6 \rightarrow l \rightarrow 5$
Refinement	
Refinement on	F^2
$R[F^2>2\sigma(F^2)]$, $wR(F^2)$, S	0.0397, 0.108, 1.101
No. of reflections and parameters used in refinement	1357, 92
H-atom treatment	Fixed
Weighting scheme	$w = 1/[\sigma^2(F_o^2) + (0.0638P)^2 + 0.1839P]$, where $P = (F_o^2 + 2F_c^2)/3$
$(\Delta/\sigma)_{max}$	0.001
$\Delta\rho_{max}$, $\Delta\rho_{min}$ (e Å^{-3})	0.272, −0.288
Extinction method	*SHELXL*97 (Sheldrick, 1997)
Extinction coefficient	0.29 (2)

Computer programs used: *Kuma KM4CCD Software* (Kuma Diffraction, 1999), *SHELXS*97 (Sheldrick, 1990), *SHELXL*97 (Sheldrick, 1997).

and the refinement for the temperature chosen are shown in Table 1. We want to emphasize that we are describing the structure in the space group $Pca2_1$, which is recommended in *International Tables for Crystallography* and thus hereafter our a, b and c parameters correspond to the b, a, c parameters of Skapski, respectively (Skapski & Stevenson, 1973). Rigid-body analysis (Cruickshank, 1956; Shomaker & Trueblood, 1968), including a non-rigidly attached rigid group (Dunitz & White, 1973; Trueblood, 1978; Dunitz *et al.*, 1988; Schomaker & Trueblood, 1998), was performed using *THMA*11 (Farrugia, 1998).

3. Results and discussion

The positional and displacement parameters of *m*-nitroaniline crystal structure at three chosen temperatures have been deposited.[1] The structures at 90 and 110 K, *i.e.* below the low-temperature anomaly, do not change compared with the structures at higher temperatures. Nevertheless, we observed some reversible changes around 130 K on the diffraction patterns of a few crystals studied. These changes indicated that the structure below 130 K became a domain one. We could resolve this structure after picking the reflections of one domain. Other crystals happened to have a one domain structure after cooling to 90 K. Their structures were resolved with better R values and the results are presented here. The R value of the structure at 340 K was higher corresponding to a high level of plasticity of the crystal. No X-ray reflections were observed at 350 K.

Fig. 2 shows the temperature dependences of the a, b, c lattice parameters of one of the specimens measured. Some discontinuities below 130 K are seen on the b and c curves. Near the (bc) plane very weak NH···O(N) intermolecular hydrogen bonds occur as well as π–π interactions. The intermolecular interactions along the a-axis direction are mainly of the van der Waals type and this is probably the reason why we do not observe any anomaly at 90 K on the a curve. All the three dependences show a drastic discontinuity above 300 K. Also the contraction of the crystal lattice along the b axis direction is well seen in Fig. 2. The anisotropic thermal expansion coefficients were calculated at 160, 200, 240 and 280 K along the crystallographic axes as well as along several other directions. The principal coefficients along the crystallographic axes at the temperatures are cited in Table 2. The α_{11} coefficient has the greatest value and it is constant in the 130–280 K temperature range. This indicates the harmonic char-

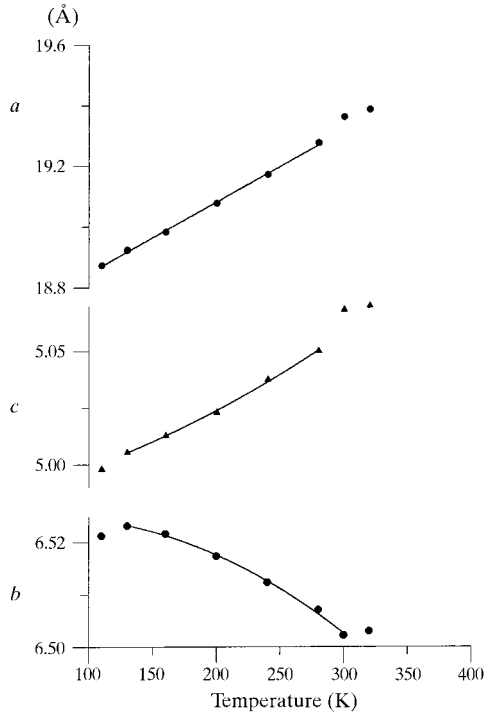

Figure 2
The temperature dependence of the *m*-nitroaniline crystal lattice parameters of one of the specimens measured. Solid lines serve as a guide to the eye.

[1] Supplementary data for this paper are available from the IUCr electronic archives (Reference: NS0004). Services for accessing these data are described at the back of the journal.

Table 2
Principal thermal expansion coefficients (deg^{-1}) at 160, 200, 240 and 280 K.

	160 K	200 K	240 K	280 K
α_{11}	1.243×10^{-4}	1.243×10^{-4}	1.243×10^{-4}	1.243×10^{-4}
α_{22}	-1.265×10^{-5}	-1.640×10^{-5}	-2.014×10^{-5}	-2.389×10^{-5}
α_{33}	5.181×10^{-5}	5.926×10^{-5}	6.672×10^{-5}	7.417×10^{-5}

$\alpha_{11} \parallel a$, $\alpha_{22} \parallel b$, $\alpha_{33} \parallel c$.

acter of interactions along the *a* direction. The stronger and anharmonic interactions on the (*bc*) plane result in the smaller and temperature-dependent value of α_{33} and the negative value of α_{22}. This is probably due to the interplay between numerous and weak interactions, mainly hydrogen bonds occurring near the (*bc*) plane. Fig. 3 shows the principal axes cross sections of the thermal expansion tensor at 160 and 280 K. The principal coefficient α_{22}, which is negative, is represented by the point in the centre of the Cartesian axes system. The anharmonicity of interactions on the (*ac*) and (*bc*) planes is well seen.

To obtain better insight into the thermal behaviour of *m*-nitroaniline we performed a rigid-body motion analysis, including the torsional motion of the nitro group. Calculations using *THMA*11 (Farrugia, 1998) provided the values of the molecular translation and libration tensors. Table 3 presents the values of the rigid-body **T**, **L** and **S** tensors in the inertial axes frame: axis 1 is lying along the long molecular axis, axis 2 is orthogonal to 1 and is lying in the molecular plane and axis 3 is orthogonal to 1 and 2 in the right-hand system of axes. The orientation of the inertial axes as well as the crystallographic ones with respect to the molecule is shown in Fig. 4. The thermal evolutions of the principal **T** and **L** values are shown in Fig. 6. It can be seen that the amplitudes of translation and libration motions grow substantially with temperature. The values of the libration amplitudes about the long molecular axis are about three times higher than the amplitudes about the two other axes. As can be seen in Fig. 4 this inertial axis lies in the (*bc*) crystallographic plane on which strongly anharmonic interactions occur. The departure of the $\mathbf{L}_{11}$ temperature dependence from the behaviour expected on the basis of harmonic potential is shown in Fig. 5. The theoretical mean-square displacement amplitudes (in deg^2) drawn as a function of temperature (broken line in Fig. 5) were calculated by fitting the Boltzmann displacement expression

$$\langle x^2 \rangle = (h/8\pi^2 Iv)\coth(hv/2kT)$$

to the lowest measured temperature (Dunitz *et al.*, 1988).

The correlation of the internal torsional motion with the overall motion (Schomaker & Trueblood, 1998) was included in the calculations and resulted in better agreement between the observed and calculated values of atomic displacements. The final weighted *R* values are shown in Table 3. This correlation enabled some kind of separation of the libration motion of the nitro group about the bisectrix of the ONO angle from the overall motion about the same axis executed by the group. The temperature dependences of the mean-square amplitudes of both motions are shown in Fig. 6.

Calculation of internal motion within the *THMA*11 program provided the mean-square amplitudes, frequencies, force constants and energetic barriers of the nitro group torsion at several temperatures. These values at 110 K are: 48.5 deg^2, 70.6 cm^{-1}, 20.2 J mol^{-1} deg^2 and 33.1 kJ mol^{-1}. The frequency of the nitro group torsion was found from IR and Raman spectra to be 94 cm^{-1} at room temperature (Szostak,

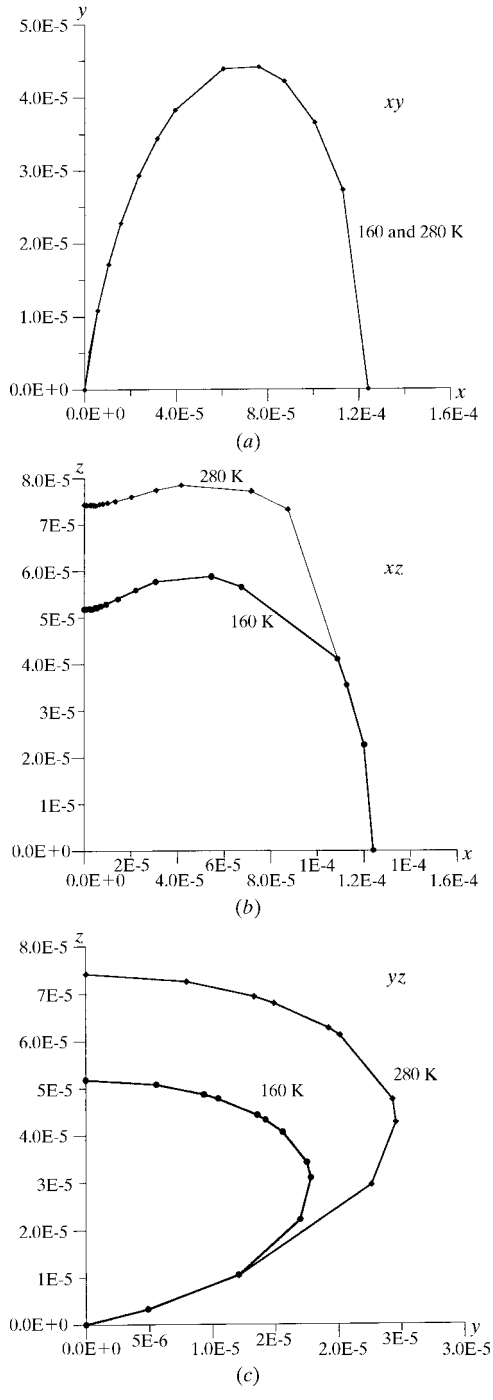

Figure 3
The principal axes cross sections of the thermal expansion tensor at 160 and 280 K. Solid lines serve as a guide to the eye.

Table 3
The values of the rigid-body **T** (Å^2), **L** (deg^2) and **S** (rad × Å) tensors at temperatures from 110 to 320 K in the inertial coordinate system.

		110 K	130 K	160 K	200 K	240 K	280 K	300 K	320 K
T (Å^2)	T^{11}	0.01509	0.01707	0.02054	0.02556	0.03122	0.03795	0.03919	0.04638
	T^{12}	−0.00049	0.00041	−0.00046	−0.00059	0.00063	0.00094	0.00085	−0.00061
	T^{13}	0.00139	0.00135	−0.00158	0.00211	−0.00231	−0.00261	0.00299	0.00180
	T^{22}	0.02013	0.02271	0.02729	0.03459	0.04248	0.05138	0.05437	0.06256
	T^{23}	−0.00189	0.00237	0.00300	−0.00405	−0.00449	−0.00509	0.00549	−0.00544
	T^{33}	0.01584	0.01624	0.02167	0.02812	0.03336	0.04104	0.04443	0.05036
L (deg^2)	L^{11}	10.760	12.074	15.377	18.935	27.303	33.954	34.793	39.900
	L^{12}	−0.386	0.484	−0.907	−0.770	1.605	1.823	1.485	−2.476
	L^{13}	−0.386	−0.690	1.062	−0.854	1.051	0.963	−0.643	−0.818
	L^{22}	2.745	3.126	4.298	5.338	7.833	9.775	10.057	13.855
	L^{23}	0.420	−0.482	−0.623	0.767	1.200	1.548	−1.576	2.333
	L^{33}	4.053	4.533	5.515	6.893	8.668	10.594	11.666	13.109
S (rad ×Å)	S^{11}	−0.00002	−0.00004	−0.00007	0.00007	0.00024	−0.00036	−0.00025	−0.00078
	S^{12}	−0.00016	0.00035	−0.00047	0.00043	0.00035	−0.00018	−0.00031	−0.00011
	S^{13}	0.00028	0.00054	−0.00067	−0.00083	−0.00147	0.00202	−0.00194	−0.00260
	S^{21}	0.00015	−0.00021	0.00020	−0.00019	−0.00031	0.00044	0.00038	−0.00027
	S^{22}	−0.00006	−0.00006	−0.00003	0.00008	−0.00040	0.00045	0.00045	0.00087
	S^{23}	−0.00047	0.00048	0.00066	0.00083	−0.00126	0.00171	−0.00172	0.00247
	S^{31}	0.00072	0.00084	−0.00100	−0.00125	−0.00143	0.00156	−0.00174	−0.00175
	S^{32}	0.00071	−0.00083	−0.00103	−0.00123	0.00166	−0.00196	0.00236	−0.00248
	S^{33}	0.00008	0.00010	0.00010	−0.00015	0.00016	−0.00010	−0.00020	−0.00010
wR†		0.062	0.062	0.051	0.051	0.046	0.042	0.040	0.044

† $wR = [\Sigma w(U_o^{ij} - U_c^{ij})^2/\Sigma w U_o^{ij2}]^{1/2}$; $w = \sigma[\langle U_o^{ij}\rangle]^{-2}$.

1982). The calculated frequencies of three translations and three librations have realistic values (30.4, 34.4, 37.3, 59.0, 70.3 and 83.5 cm^{-1} at 110 K) and realistic temperature dependences. The non-standard temperature behaviour at the lowest and highest temperatures probably reflects the singularities of the thermal expansion.

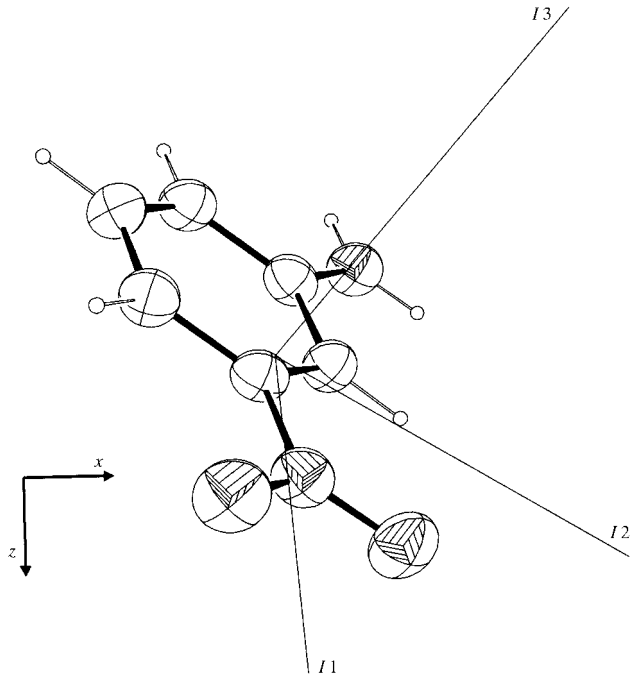

Figure 4
The orientation of the inertial axes as well as the crystallographic ones with respect to the *m*-nitroaniline molecule.

Detailed analysis of the short intermolecular distances at various temperatures showed that the distances corresponding to weak NH···O(N), CH···O and NH···N hydrogen bonds are evolving with increasing temperature far weaker than other intermolecular distances and even exhibit some contraction, as shown in Table 4. This probably reflects the growing amplitudes of the librational and torsional motions in which the amino and nitro groups are involved. It also seems to indicate that hydrogen bonds are preserved in the high-temperature phase. On the other hand, the molecular dynamics, represented here by the values of the **T** and **L** tensor coefficients, grow considerably with temperature. Such a behaviour may be rationalized in terms of the growing reorientations of molecular aggregates formed by hydrogen-bonded molecules. This presumption is consistent with our previous dielectric results, which indicated the onset of reorientations of large molecular aggregates from above room temperature coupled with growing electric conductivity (Szostak *et al.*, 1998). The molecular aggregates can correspond to molecular strands described by Turi & Dannenberg (1996).

4. Conclusions

The presented investigation into the *m*-nitroaniline crystal structure over a wide temperature range shows the anharmonicity of molecular interactions on the *bc* plane. The transformation of an *m*-nitroaniline crystal to a plastic phase near 340 K seems to be confirmed. Also, the dilatometric singularities observed at ∼130 K are in line with the differential scanning calorimetry (DSC) anomalies at a similar

Table 4
Short intermolecular distances in *m*-nitroaniline at various temperatures.

T (K)	N2$^{i}\cdots$O2^{ii}	N2$^{i}\cdots$O2^{iii}	N2$^{i}\cdots$O1^{ii}	N2$^{i}\cdots$N2^{iv}	O1$^{ii}\cdots$C 4^{i}	O2$^{i}\cdots$C5^{v}
90	3.237	3.295	3.369	3.237	3.328	3.549
140	3.247	3.314	3.416	3.254	3.335	3.574
180	3.253	3.319	3.427	3.264	3.346	3.599
220	3.262	3.336	3.429	3.281	3.344	3.615
260	3.279	3.345	3.441	3.302	3.358	3.644
302	3.266	3.330	3.460	3.306	3.360	3.674
340	3.257	3.326	3.448	3.324	3.353	3.691

Symmetry codes: (i) x, y, z; (ii) $x, y-1, z-1$; (iii) $\frac{1}{2}-x, y-1, z-\frac{1}{2}$; (iv) $\frac{1}{2}-x, y, z+\frac{1}{2}$; (v) $x, y, z+1$.

temperature. The two transitions need separate discussions. The low-temperature effect looks like a glass transition on the DSC curves. Such a transition was found recently in *p*-chloronitrobenzene and was interpreted as originating possibly from freezing the nitro group torsional motion (Meriles *et al.*, 1996; Tozuka *et al.*, 2000). In the case of *m*-nitroaniline, the freezing rather concerns the libration and translation motions of the whole molecule, because the torsional motion amplitude is still high at 110 K. We would correlate the transition also with the elongation of the crystal lattice along the *b*-axis direction with decreasing temperature. Such an anomaly of thermal expansion provokes a stress followed by a strain, which may lead to some kind of 'catastrophe', resulting in partition of a single crystal into several domains. The transition is reversible, so this must be an equilibrium process. Thus, the DSC effect seems to correspond to macroscopic changes of crystal structure. Nevertheless, we would like to mention the phase transitions in polyphenyls, which occur at temperatures between 80 and 250 K (depending on the number of phenyls) and are connected with freezing of torsional motions of benzene rings about the long molecular axis (Toudic *et al.*, 1987). This freezing leads to superstructures and results in doubling of one of the unit-cell lengths. The molecules in *m*-nitroaniline crystal form molecular chains along the [*bc*] diagonal owing to weak hydrogen bonds. This time, however, the freezing of molecular vibrations does not lead to any superstructure.

As to the high-temperature effect, we think that this is a second-order phase transition to a plastic phase in which the molecules exhibit a high level of reorientational freedom. This transformation seems to be driven by librational motion about a long molecular axis coupled with growing torsional vibrations of the nitro group. Yet the hydrogen bonds seem to stay preserved, at least to some extent, in the plastic phase forming molecular aggregates which exhibit considerable reorientations. All this seems to indicate that the crystallization process from the melt must start with forming aggregates of hydrogen-bonded molecules and then, with decreasing temperature the aggregates pack to form a crystal seed.

This work was sponsored in part by Wrocław University of Technology within the 341763 program.

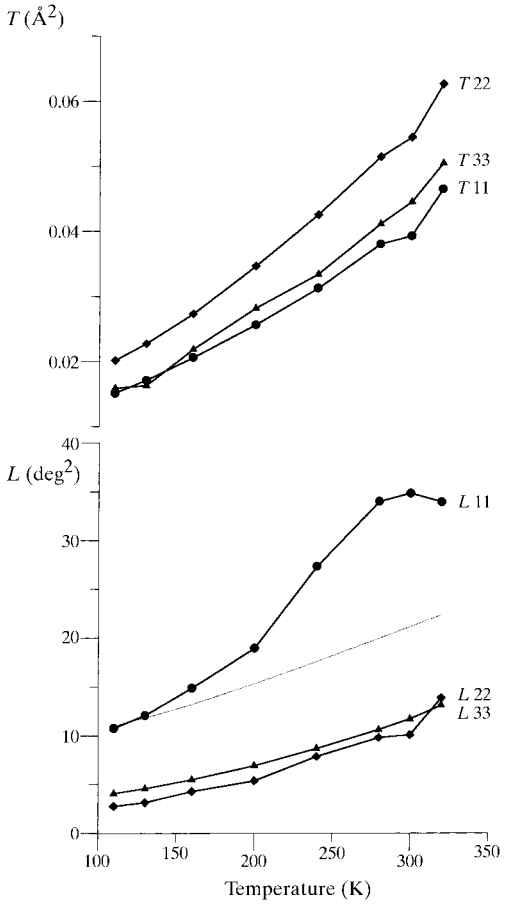

Figure 5
Thermal evolution of the principal values of the **T** and **L** tensors. Solid lines serve as a guide to the eye. The dotted line is a theoretical fit of $\mathbf{L}_{11}$ temperature dependence based on the harmonic potential. For details see text.

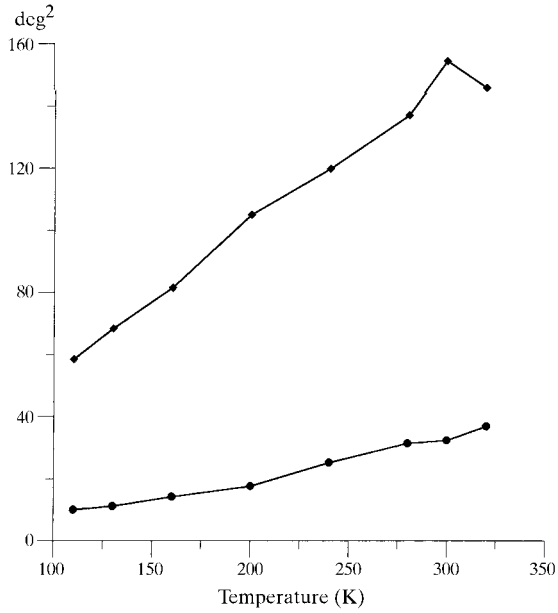

Figure 6
Temperature dependence of the amplitudes of the nitro group motion. The upper dependence relates to the overall motion about the bisectrix of the ONO angle. The lower dependence relates to the libration motion about the same axis. Solid lines serve as a guide to the eye.

References

Allen, F. H., Baalham, C. A., Lommerse, J. P. M., Raithby, P. R. & Sparr, E. (1997). *Acta Cryst.* B**53**, 1017–1024.

Allen, F. H., Lommerse, J. P. M., Hoy, V. J., Howard, J. A. K. & Desiraju, G. R. (1997). *Acta Cryst.* B**53**, 1006–1016.

André, I., Foces-Foces, C., Cano, F. H. & Martinez-Ripoll, M. (1997*a*). *Acta Cryst.* B**53**, 984–995.

André, I., Foces-Foces, C., Cano, F. H. & Martinez-Ripoll, M. (1997*b*). *Acta Cryst.* B**53**, 996–1005.

Asaji, T. & Weiss, A. (1985). *Z. Naturforsch. Teil A*, **40**, 567.

Cruickshank, D. W. (1956). *Acta Cryst.* **9**, 754–756.

Davidov, B. L., Derkaceva, L. D., Dunina, V. V., Zhabotinskii, M. E., Zolin, B. F., Koreneva, L. G. & Samochina, M. A. (1970). *Zh. Exp. Teor. Fiz.* **12**, 24.

Dunitz, J. D., Maverick, E. F. & Trueblood, K. N. (1988). *Angew. Chem. Int. Ed. Engl.* **27**, 880–895.

Dunitz, J. D. & White, D. N. J. (1973). *Acta Cryst.* A**29**, 93–94.

Farrugia, L. (1997). *J. Appl. Cryst.* **30**, 565.

Farrugia, L. (1998). *WinGX-A*. University of Glasgow, Scotland.

Giermańska, J. (1984). Ph.D. Thesis, Wrocław, Poland.

Goeta, A. E., Howard, J. A. K., Ellena, J., Punte, G., Autino, J. C. & Wilson, C. C. (1999). *Proc. XVIIIth IUCr Congress*, Glasgow 1999, p. 402.

Höhne, G., Hemminger, W. & Flammersheim, H.-J. (1995). *Differential Scanning Calorimetry*. Berlin: Springer-Verlag.

Kuma Diffraction (1999). *Kuma KM4CCD Software.* Version 1.61. Kuma Diffraction, Wrocław, Poland.

Meriles, C. A., Perez, S. C. & Brunetti, A. H. (1996). *Phys. Rev. B*, **54**, 7090–7093.

Panunto, T., Urbańczyk-Lipkowska, Z., Johnson, R. & Etter, M. C. (1987). *J. Am. Chem. Soc.* **109**, 7786–7797.

Ploug-Sørensen, G. & Krogh Andersen, E. (1986). *Acta Cryst.* C**42**, 1813–1815.

Sheldrick, G. M. (1990). *Acta Cryst.* A**46**, 467–473.

Sheldrick, G. (1997). *SHELX*97. University of Göttingen, Germany.

Shomaker, V. & Trueblood, K. N. (1968). *Acta Cryst.* B**24**, 63–76.

Shomaker, V. & Trueblood, K. N. (1998). *Acta Cryst.* B**54**, 507–514.

Skapski, A. C. & Stevenson, J. L. (1973). *J. Chem Soc. Perkin Trans. 2*, pp. 1197–1200.

Southgate, P. D. & Hall, D. S. (1971). *Appl. Phys. Lett.* **18**, 456–458.

Szostak, M. M. (1979). *J. Raman Spectrosc.* **8**, 43–49.

Szostak, M. M. (1982). *J. Raman Spectrosc.* **12**, 228–233.

Szostak, M. M. (1988). *Chem. Phys.* **121**, 449–456.

Szostak, M. M., Jakubowski, B. & Komorowska, M. (1993). *Mol. Cryst. Liq. Cryst.* **229**, 7–10.

Szostak, M. M., Le Calve, N., Romain, F. & Pasquier, B. (1994). *Chem. Phys.* **187**, 373–380.

Szostak, M. M., Wójcik, G., Gallier, J., Berteault, M., Freundlich, P. & Kołodziej, H. A. (1998). *Chem. Phys.* **229**, 275–284.

Toudic, B., Cailleau, H., Lechner, R. E., Gallier, J., Petry, W. & Perrin, D. (1987). *Dynamics of Molecular Crystals*, edited by J. Lascombe, p. 529. Amsterdam: Elsevier.

Tozuka, Y., Yamamura, Y., Saito, K. & Sorai, M. (2000). *J. Chem. Phys.* **112**, 2355–2360.

Trueblood, K. N. (1978). *Acta Cryst.* A**34**, 950–954.

Turi, L. & Dannenberg, J. J. (1996). *J. Phys. Chem.* **100**, 9638–9648.